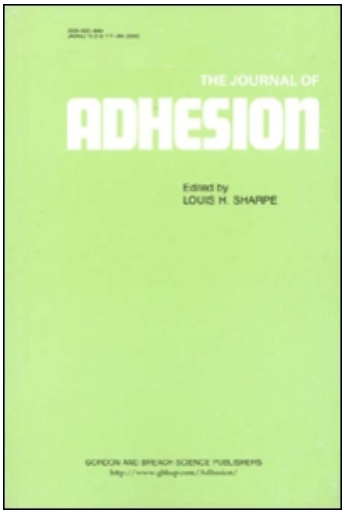

The Journal of Adhesion
Publication details, including instructions for authors and subscription information:
http://www.informaworld.com/smpp/title~content=t713453635

Stress Transfer Function for Interface Assessment in Composites with Plasma Copolymer Functionalized Carbon Fibres

N. Lopattananon[a]; S. A. Hayes[a]; F. R. Jones[a]
[a] Department of Engineering Materials, University of Sheffield, Sheffield, United Kingdom

Online publication date: 08 September 2010

To cite this Article Lopattananon, N. , Hayes, S. A. and Jones, F. R.(2002) 'Stress Transfer Function for Interface Assessment in Composites with Plasma Copolymer Functionalized Carbon Fibres', The Journal of Adhesion, 78: 4, 313 — 350
To link to this Article: DOI: 10.1080/00218460210935
URL: http://dx.doi.org/10.1080/00218460210935

The Journal of Adhesion, 78: 313–350, 2002

0021-8464/02 $12.00 +.00

STRESS TRANSFER FUNCTION FOR INTERFACE ASSESSMENT IN COMPOSITES WITH PLASMA COPOLYMER FUNCTIONALIZED CARBON FIBRES

N. Lopattananon, S. A. Hayes, and F. R. Jones
Department of Engineering Materials, University of Sheffield, Sheffield, United Kingdom

Radio-frequency-induced plasma copolymerization of acrylic acid/1,7-octadiene was used to produce a range of functionalized plasma copolymer coatings with controlled degree of adhesion. The single-fibre fragmentation test was used to characterize the adhesion of plasma copolymer coated fibres to epoxy resin. The cumulative stress transfer function (CSTF) and Kelly-Tyson approaches were used to evaluate the degree of adhesion. By continuous monitoring of the fragmentation process, it was found that the mechanical performance of a composite material could be evaluated using the CSTF methodology at strain well below saturation. The degree of debonding was a good measure of relative interface/interphase adhesive strength. The trend in the CSTF is consistent with the propagation of interfacial debonds during the test. For a completely debonded fibre a normalized CSTF value, referred as stress transfer efficiency (STE), was found to provide a more consistent analysis that was able to differentiate between fibres with similar degrees of debonding. The calculated values of interfacial shear strength (IFSS) were only valid for a fully debonded fibre (1,7-octadiene plasma homopolymer coating) where the assumption of a constant shear stress, as in the Kelly-Tyson model, applied. However, IFSS did not provide the same ranking. Where debonding does not occur, the stress transfer efficiency also provides a sensitive measure of the interface/interphase performance. Improved adhesion over the untreated-unsized carbon fibre was observed for both of the plasma copolymer-coated and commercially treated carbon fibres. Since there is a concentration dependence of carboxyl groups on adhesion, the mechanism appears to relate to covalent bond formation with the epoxy group. Plasma copolymer coatings on carbon fibres also causes an increased tensile strength and Weibull modulus.

Keywords: Fragmentation test; Adhesion mechanisms; Plasma polymerization; CSTF methodology; Kelly-Tyson model; Shear stress transfer

Received 5 May 2001; in final form 10 December 2001.

N. Lopattananon gratefully acknowledges the Thai government for financial support. We also acknowledge funding by EPSRC (to S. A. Hayes). The work has been carried out in conjunction with the European Network on Interphases.

Address correspondence to F. R. Jones, Department of Mechanical Engineering, University of Sheffield, Sir Robert Hatfield Building, Mappin Street, Sheffield S1 3JD, UK. E-mail: f.r.jones@sheffield.ac.uk

INTRODUCTION

Carbon-fibre-reinforced polymer composites are used in a wide range of industrial applications. An important factor which determines the performance of the carbon fibre-reinforced polymers is the quality of fibre-matrix interfacial adhesion. Carbon-fibres are always surface treated to provide an improvement to their adhesion. In addition, they are coated with a polymer, i.e., size, to protect from handling damage and to aid processability. The nature of the physical and chemical interactions between the treated carbon fibre, the size, and the resin matrix leads to the formation of either an interface or an interphase [1, 2]. This is a region where the applied load is transferred to the reinforcing fibre. Whether an interface or interphase forms, its mechanical properties are a function of surface chemistry. With conventional surface treatment, i.e., electrochemical oxidation, the mechanisms of fibre-matrix adhesion have not yet been fully identified. Various mechanisms have been proposed; the formation of covalent bonds [3, 4], mechanical keying [5], physical adsorption of the resin molecule or their segment into micropores [6], and the removal of contaminants such as weakly-bonded crystallites [7]. Furthermore, one or more of these mechanisms may contribute to adhesion. Denison et al. [6] have demonstrated that the increase in load-bearing capability of composites may be linked to the increased concentration of chemical functional groups and/or broadening of surface microporosity on the treated surface. However, a successful attempt to resolve the differing contributions of chemical functionality and surface microporosity using conformal plasma polymer coatings which conceal the residual structure and provide controllable surface chemistry has been made [8]. Furthermore, the conformal nature of the coating which provides the protection from damage is reported [9–11].

The single-fibre fragmentation test has been widely used to characterize the mechanical properties of the interface because it provides a means of assessing the effect of surface treatment on the differing interfacial shear strengths in carbon and glass fibre composites [12, 13]. The single-fibre fragmentation test relies on applying a tensile force to a specimen with a single embedded fibre in a thin resin test piece. The tensile stress is transmitted to the fibre through an interfacial shear stress until it is high enough to cause fracture. Subsequently, as the applied strain increases, the fibre breaks repeatedly at points where the fibre strength is exceeded. Continued application of load results in further fragmentation until the length of the remaining fragments is no longer sufficient for further fracture to occur. This

situation is defined as the saturation in the fibre fragmentation process. The final fragment lengths in a transparent matrix composite can be measured using an optical microscope. However, the assumption of a constant interfacial shear stress in the analytical model which is currently used [14] is unrealistic where only partial debonding occurs. Thus, the values of interfacial shear strength (IFSS) obtained from the fragmentation test are not always consistent. The problems arise from the complexity of the phenomena occurring during the fragmentation process [15, 16]. Therefore, an alternative approach for the evaluation of fibre-matrix adhesion was developed by Tripathi and Jones [17], which takes into account the properties of this matrix. In particular, the elastic, elastic-plastic stress and frictional components of stress transfer are included.

Models for Estimating Interfacial Adhesion Parameters

The Constant Shear Model

The constant shear model of Kelly and Tyson [14] uses a force balance argument to determine the efficiency of the interface to transfer stresses, τ_a:

$$\tau_a = \frac{\sigma_{fu} d}{2 l_c}, \tag{1}$$

where d is the fibre diameter and σ_{fu} is the fibre strength at a length equal to the critical fibre length, l_c. A value of l_c can be calculated by using Ohsawa's relationship [18]:

$$l_c = \frac{4\bar{l}}{3}, \tag{2}$$

where $\bar{l}$ is the average fragment length.

The estimate of σ_{fu} can be derived from the Weibull modulus (m) and average fibre strength at given gauge length.

The Cumulative Stress Transfer Function (CSTF) Approach

The cumulative stress transfer function (CSTF) [17] is a technique for assessing fibre-matrix adhesion from the single-fibre fragmentation test. It is assumed that a better interface transfers a higher fraction of the applied load, so that an estimate of the tensile stress profile in a fragmented filament would be a good measure of the efficiency of an interface. The CSTF value can be defined as follows:

$$\mathrm{CSTF} = \frac{\sum_{i=1}^{i=N} \int_0^{L_i} \sigma_f(x)dx}{\sum_{i=1}^{i=N} L_i}, \tag{3}$$

where N is the number of fragments of length L_i, where $i = 1, 2, 3 \cdots N$, x is the distance along the fibre-end, and $\sigma_f(x)$ is the tensile stress at a distance x from the fibre-end. The CSTF technique employs the plasticity effect model of Tripathi et al. [19] to predict the tensile stress profile in the fibre fragment from measurement of bonded and debonded lengths. For the elastic-plastic stress component, a Von Mises yield criterion is included. Therefore, the calculated tensile stress profile is a function of fibre and matrix properties, the stress state of the specimen and associated yielding and/or debonding features.

The Plasticity Effect Model

This model [19] is a simple approach for introducing the effect of matrix plasticity into a stress transfer model numerically, without the need for finite element analysis. In effect, the shear stress transfer profile in the elastic matrix/elastic fibre region is calculated from the variational model [20] according to Equation (4) and interrupted for shear yield by applying a von Mises yield criterion to the matrix stress at the interface. A more complex yield criterion would refine the yield point but it is within the uncertainty in the fragmentation process.

$$[\sigma_f] = [B_1][\psi] \tag{4}$$

Where

$$[\sigma_f] = (\sigma_{rr}, \sigma_{\theta\theta}, \theta_{zz}, \tau_{rz})$$

$$[\psi] = [\sigma(p), T, \psi, \psi^{\mathrm{I}}, \psi^{\mathrm{II}}, \sigma_\infty]$$

$$[B_1] = \begin{bmatrix} -\frac{V_m A_4}{V_f A_o} & -\frac{V_m A_5}{V_f A_o} & -\frac{V_m A_3}{V_f A_o} & 0 & f_1 & V_f\left(1 - \frac{V_m A_2}{V_f A_o}\right) \\ -\frac{V_m A_4}{V_f A_o} & -\frac{V_m A_5}{V_f A_o} & -\frac{V_m A_3}{V_f A_0} & 0 & f_2 & V_f\left(1 - \frac{V_m A_2}{V_f A_o}\right) \\ 0 & 0 & 1 & 0 & 0 & 0 \\ 0 & 0 & 0 & -\frac{1}{2}\xi & 0 & 0 \end{bmatrix}$$

$\sigma_{zz}, \sigma_{rr}, \sigma_{\theta\theta}$, and τ_{rz} are the tensile stresses in the fibre, the radial, hoop, and shear stresses at the fibre interface, respectively. T is the stress free or cure temperature. The other constants are geometrical and material properties. Typical values are given in Table 1.

The variational model was chosen because it provided the closest prediction to our elasto-plastic finite element model [21] and provides

TABLE 1 Fibre and Epoxy Resin Matrix Properties Used in the Calculation of CSTF Values [23]

Material properties	Value
Longitudinal elastic modulus of fibre (Gpa)	238
Transverse elastic modulus of fibre (Gpa)	14
Longitudinal Poisson's ratio of the fibre	0.20
Transverse Poisson's ratio of the fibre	0.25
Longitudinal shear modulus of fibre (Gpa)	20
Friction coefficient	0.20
Fibre volume fraction	0.001
Longitudinal thermal expansion coefficient of fibre (K^{-1})	-0.1×10^{-6}
Transverse thermal expansion coefficient of fibre (K^{-1})	18×10^{-6}
Thermal expansion coefficient of matrix (K^{-1})	40×10^{-6}
Shear yield strength of matrix (Mpa)	31.8
Shear cold draw strength of matrix (Mpa)	21

an estimate of radial stresses required for debonded regions. In this way, a complete shear stress profile can be calculated for each fragment in the test specimen at any applied strain, taking into account elastic-elastic stress transfer in the bonded unyielding region and frictional (through Coulomb's law) within debonded regions, as shown in Figure 1a.

From the shear stress profile, the axial fibre stress profile in each fragment can be calculated, as shown in Figure 1b.

The stress transfer function (STF) for each fragment can thus be calculated by integrating axial fibre-stress profile. CSTF is then obtained by summing the contributions of each fragment in the specimen gauge length and normalizing to the total length of the fragments, according to Equation (3).

It will be shown that for fully debonded fibres where fragmentation has ceased it is more appropriate to consider stress transfer efficiency (STE) function. This can be obtained by calculating a normalizing factor for stress transfer under ideal elastic-elastic conditions from the variational model [20]. According to Nairn's model [20], bonding between fibre and matrix is assumed to be perfect. Therefore, it is possible to calculate the average tensile stress carried by fibres of different average lengths and each level of applied strain under ideal elastic conditions. This provides the calibration curve for the calculation of a stress transfer efficiency for fibres of the same length at a specific strain. The calibration curve for the untreated-unsized carbon

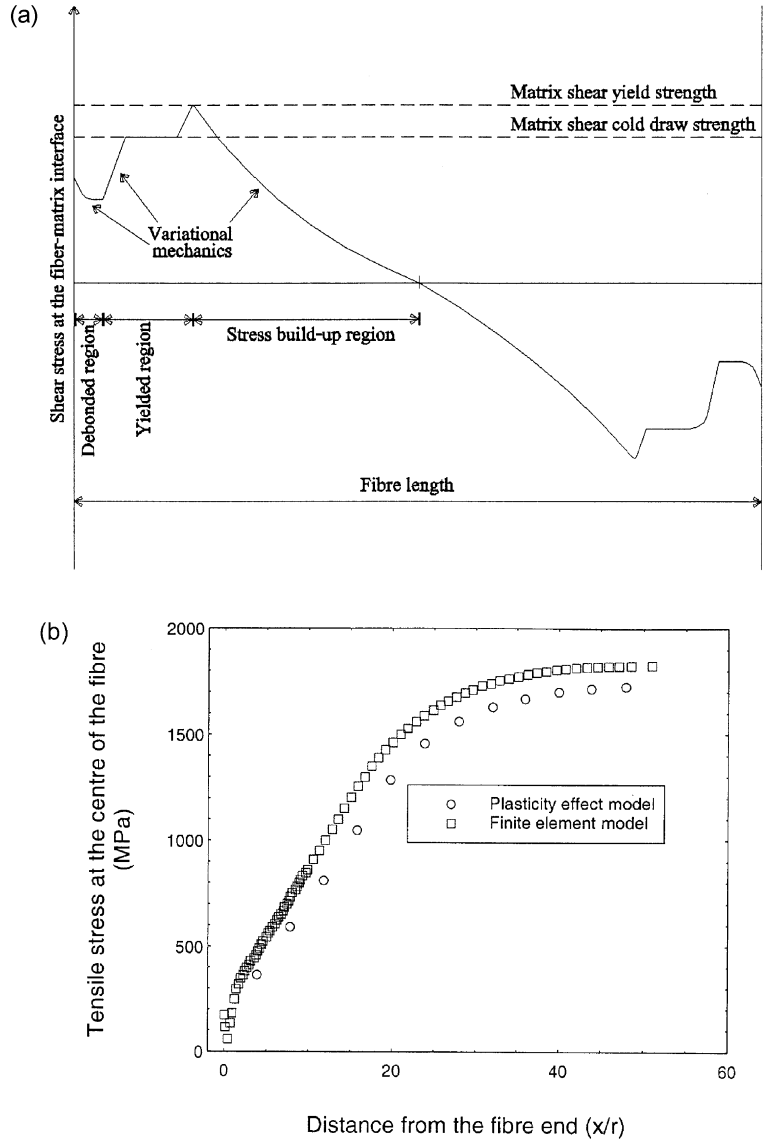

FIGURE 1 (a) Schematic of the shear stress profile obtained from the Plastic Effect Model [19] illustrating the use of the Variational Model [20]. (b) Comparison of the tensile stresses at the center of an embedded carbon fibre at an applied strain of 3%, predicted by the Plasticity Effect Model (o) and the Finite Element Model (□) [19].

fibres with a diameter of 7.53 μm are shown in Figure 2. It can be seen that the average stress transferred to a fibre, determined from Nairn's equation, increases with fibre length and applied strain. This provides a means of obtaining a STE, which is expressed as follows:

$$\mathrm{STE} = \frac{\mathrm{CSTF}}{\overline{\sigma}_f} = \frac{\mathrm{CSTF}}{[\mathrm{CSTF}]^0}, \tag{5}$$

where STE is the stress transfer efficiency and $\bar{\sigma}_f$ is average tensile stress in the fragments under ideal elastic conditions, obtained from the calculated profiles in an analogous manner to CSTF and represents $[\mathrm{CSTF}]^0$, which is the magnitude of the ideal stress transferred by a fragment. Thus, the shear stress profile in Figure 1b is not interrupted for matrix yield nor fibre-matrix debonding.

The main objective of this study is to examine the conventional and CSTF methodologies for interpretation of the single-fibre fragmentation test data. The correlation between the CSTF and STE and the chemistry of plasma copolymerized fibres was evaluated and compared

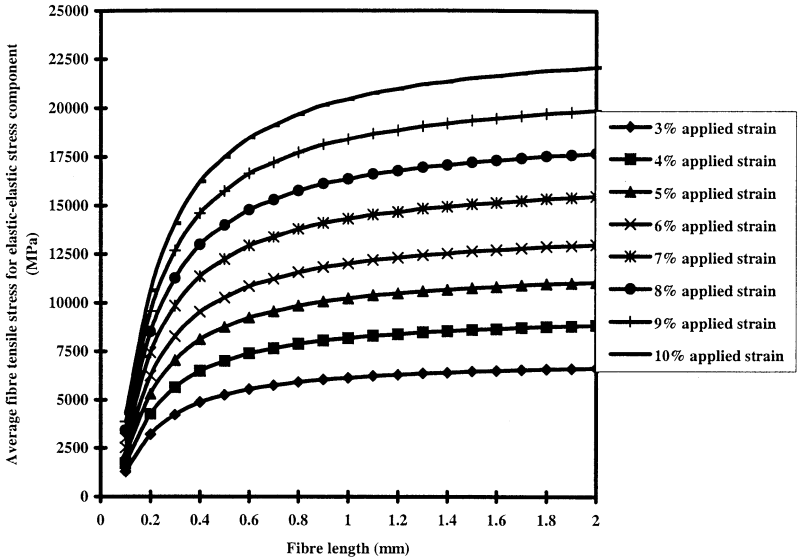

FIGURE 2 Average fibre tensile stress for elastic-elastic stress conditions calculated from the Nairn Model [20] with average fragment length at increments of applied strain. The data are for the untreated-unsized (HTA-5000) carbon fibres which are representative of a fibres with a diameter (d_f) of 7.53 μm.

with estimates of IFSS obtained from the conventional constant shear model. Radio-frequency-induced plasma polymerization was used to deposit a range of conformal, pinhole-free, highly-adhering, cross-linked polymeric coatings with differing concentration of various functional groups. The chemical structure and composition of the plasma polymer coatings were characterized using XPS. Scanning electron microscopy (SEM) was used to study the morphology of the plasma polymer coated fibres.

EXPERIMENTAL

Fibre and Plasma Polymer Coatings

Untreated, unsized Type A carbon fibre (Tenax HTA-5000), treated, unsized (Tenax HTA-5001) and treated, sized (Tenax HTA-5131) carbon fibres were used in this study. Radio-frequency plasma copolymerization of acrylic acid/1,7-octadiene was performed in a cylindrical, glass reactor 50×10 cm in diameter. Acrylic acid was chosen because the degree of adhesion to epoxy resin can be controlled by the introduction of carboxylic acid groups [8, 22]. All monomers were supplied by Aldrich Chemical Co., UK, at 99% purity or above. Single fibres were extracted randomly from the untreated-unsized (HTA-5000) fibre tow and adhered to wire frame supports. At least 15 frames, approximately 10 cm in length, were suspended on a frame holder which was then placed within the plasma reactor. A series of four coatings were prepared ranging from hydrocarbon to highly functional. This was done by regulating the mole fraction of a hydrocarbon and acrylic acid comonomer independently in the plasma feed while maintaining a constant total monomer flow rate (F) and plasma power (P). The detailed summary of plasma parameters for coatings is given in Table 2. A detailed deposition procedure and the plasma apparatus have been described elsewhere [22]. A highly functionalized coating produced from the deposition of the acrylic acid onto treated-unsized carbon fibre (HTA-5001) (see Table 2) was also studied.

TABLE 2 Summary of Coating and Plasma Parameters for the Single-fibre Fragmentation Test

Monomer composition	Total flow rate (sccm)	Plasma power (W)	Polymerization time (min)
Acrylic acid-1,7-octadiene	1.5	5	15
Acrylic acid	1.5	0.7	15

X-ray Photoelectron Spectroscopy (XPS)

An aluminium foil substrate was placed within the radio-frequency chamber alongside the carbon fibres to provide a suitable plasma polymer sample for analysis by X-ray photoelectron spectroscopy (XPS). The XPS spectra were performed using a VG Clam 2 X-Ray Photoelectron Spectrometer operating in constant analyzer energy mode with a dual anode utilizing MgKα X-rays as the X-ray source at a power of 100 W. Analysis was performed at a take-off angle of 30° with respect to the sample surface. This was to provide the XPS analysis depth within approximately 5 nm from the surface of the plasma polymer coating. The core-level spectra of all regions of interest (carbon and oxygen core levels) were recorded to determine the elemental composition of the plasma polymer surface coatings. Curve fitting of the core-level spectra was performed to provide the chemical environment of the various carbon-containing groups using a least squares routine which, in an iterative manner, optimizes the parameters which define the several component peaks contained within the experimental spectral envelope.

Scanning Electron Microscope (SEM)

The changes in fibre surface topography following plasma polymer deposition were characterized using a Jeol 6400 SEM scanning electron microscope (SEM).

Resin Matrix

The resin matrix was obtained by blending Epikote 828 (Shell Chemicals, London, UK) with flexibilizer, Araldite GY 298 (Ciba Geigy, Duxford, UK) in the ratio of 63 parts to 37, respectively. This was cured with 70 phr nadic methyl anhydride (Stag Polymers and Sealants, London) and Capcure 3-800 (Henkel-Nopco, Leeds, UK), a mercaptan-terminated polymer. The matrix was subsequently cured at 55°C for 18 h, postcured at 13°C for 3 h, followed by cooling in the oven. The resulting resin had an elastic modulus of 3 GPa and a tensile yield strength of 55 MPa. By way of the von Mises relationship, a shear yield strength of 31.8 MPa was calculated from the value of the tensile yield strength.

Fragmentation Test Technique

The test uses a specimen which has a single fibre embedded longitudinally in a resin with a strain to failure to achieve saturation in the

fragmentation process (an applied strain of 10% has often been required). Full details of the experimental procedure and sample preparation for the fragmentation test have been given in previous papers [2]. The fragmentation test was performed using a minitensile tester (Micromaterials Limited, Wrexham, UK). Test specimens were subjected to a uniaxial tension at a displacement rate of 0.13 mm/min. The fragmentation test was interrupted at increments of applied strain and all of the fragments and associated interfacial failure processes near the fibre fractures were digitized and recorded for subsequent analysis. An initial strain of 3% was chosen because it produced only limited fibre fracture. The test was stopped after the sample elongation had reached an applied strain of 10%. From the digitalized micrographs obtained during the test the fragment and debond lengths at each level of applied strain can be measured. A custom-written Visual basic program enables the fibre breaks to be identified so that the debonded and bonded lengths can be measured with a simple click of the mouse. The magnification is included through a calibration using a known graticule. Full details of the experimental set-up, software, and experimental procedure are given elsewhere [23]. The tensile strengths of the fibres were measured at a gauge length of 6.25 mm, according to the procedure described by Cheng et al. [2]. Weibull modulus was estimated using the maximum likelihood method described by Cheng et al. [2]. Fibres with a commercial treatment through electrolytic oxidation with and without sizing were also studied for comparison.

RESULTS

XPS Analysis of Plasma Polymer Coatings

The surface chemical composition of plasma copolymer coatings from acrylic acid and 1,7-octadiene deposited onto untreated-unsized and treated-unsized fibres is given in Table 3. It can be seen from Table 3 that the deposition of a plasma polymer from acrylic acid produces the highest concentration of carboxylate (COOR) functional groups on the fibre surfaces. Previous work has shown that, under the plasma conditions employed, about 80% of the COOR group is retained and it is principally COOH [24]. Furthermore, the high retention of carboxylic acid groups is confirmed by the relative peak areas of COOR and C-COOR. The concentration of COOR groups decreases with the dilution by 1,7-octadiene. It is apparent from Table 3 that the concentration of carboxylate functionalities retained in the plasma homopolymers of acrylic acid at lower (0.7 W) and higher (5.0 W) power was not

TABLE 3 XPS Analysis for the Plasma Polymer Coatings

Coating parameters			% Chemical functionalities of C1s core level				
Monomer composition	Hydrocarbon (mole fraction)	% O/C	COOR	COR	C=O	C-R	C-COOR
Untreated-unsized	—	—	—	—	—	92.1	—
	0	0.44	17.7	7.3	3.1	54.4	17.7
Acrylic acid/ 1,7-octadiene (5 W, 1.5 sccm and 15 mins)	0.25	0.25	7.5	10.1	3.4	71.9	7.5
	0.50	0.09	2.0	7.9	0.7	89.5	2.0
	1.0	0.02	0	2.9	0	97.5	
Acrylic acid (0.7 W, 1.5 sccm and 15 mins)	0	0.52	19.6	5.2	2.9	52.8	19.6

significantly different. The apparent insensitivity to plasma power can be attributed to the use of a differing reactor.

Scanning Electron Microscopy (SEM)

A SEM micrograph showing the coating layer on carbon fibre is given in Figure 3. For a series of plasma-copolymer-coated fibres, SEM micrographs indicated that coating thickness was approximately 200−300 nm. The fibre diameters for untreated-unsized (HTA-5000), treated-unsized (HTA-5001), and treated-sized (HTA-5131) carbon fibres are given in Table 4.

Tensile Strength Measurement

The results of measured average tensile strength and Weibull modulus (m) of the plasma-polymer-coated fibres are given in Table 4. There is an apparent trend of an increase in strength of the uncoated fibres (HTA-5000) after plasma copolymer deposition, which is dependent on the mole fraction of acrylic acid. The strength of the 1,7-octadiene plasma-polymer-coated fibres is identical to that of the precursor. Furthermore, the strengths of the fibres coated with the acrylic acid plasma polymer at high (5.0 W) and low power (0.7 W) were similar. A similar result was reported previously [22]. The statistical distribution in fibre strength leads to a large standard deviation, which makes it difficult to identify the true significance. However, it is

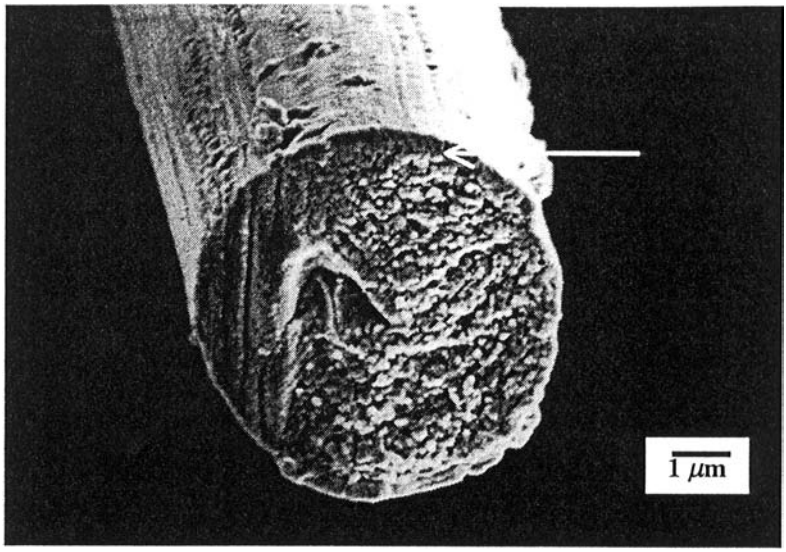

FIGURE 3 Typical scanning electron micrograph of a coating layer for plasma-polymer-coated carbon fibre. Arrow indicates the plasma polymer coating layer.

generally accepted that polymer sizing does play a role, as shown by the data for HTA 5131. A better way of assessing any improvement in strength is through the Weibull modulus (m), which is a measure of the width of the distribution. Thus, the higher the value of m, the narrower the distribution in strength.

Examination of the series of plasma-polymer-coated untreated-unsized fibres (HTA-5000 in Table 4) shows that the Weibull modulus (m) increases steadily with the polarity of the plasma polymer, approaching the value for the treated-sized fibre (HTA-5131). All of the fibres were handled in an identical manner, so it can be concluded that the trend may well be significant.

Fragmentation Test Results

Fragmentation Process of Plasma-Polymer-Coated Fibres with Acrylic Acid/1,7-Octadiene

The fragmentation process for each of the plasma-polymer-coated fibres prepared from acrylic acid and 1,7-octadiene was continuously monitored. The fragmentation test data are summarized in Table 5. The variation in the number of fragments/10 mm or fragment number,

TABLE 4 Tensile Strength of Plasma-polymer-coated Carbon Fibres: Untreated-unsized (HTA-5000), Treated-unsized (HTA-5001), Treated-sized (HTA-5131), and HTA-5000 with Plasma Poly(acrylic acid-co-1,7-octadiene) Coatings

		Coating parameters		Fibre parameters				
Fibre	No. of samples	Monomer composition	Acrylic acid (mole fraction)	Diameter (μm)	Strength (GPa)	Failure strain (%)	Modulus (GPa)	Weibull modulus (m)
HTA-5000	63	—	—	7.53 ± 0.33	3.60 ± 1.09	1.66 ± 0.59	223 ± 47	3.62
HTA-5001	70	—	—	7.20 ± 0.20	3.65 ± 0.93	1.78 ± 0.49	216 ± 49	4.67
HTA-5131	88	—	—	7.17 ± 0.49	4.46 ± 0.84	1.93 ± 0.48	241 ± 45	5.61
HTA-5000	79	Acrylic acid/	0	—	3.72 ± 1.36	1.62 ± 0.70	240 ± 55	3.02
	70	1,7-octadiene	0.50	—	4.10 ± 1.17	1.81 ± 0.54	236 ± 56	3.93
	72	(5.0 W, 1.5 sccm	0.75	—	4.26 ± 1.07	1.91 ± 0.51	231 ± 45	4.53
	67	and 15 min)	1.0	—	4.27 ± 0.85	2.12 ± 0.62	218 ± 53	5.42
HTA-5001	60	Acrylic acid (0.7 W, 1.5 sccm and 15 min)	1.0	—	4.16 ± 0.89	2.15 ± 0.57	205 ± 58	5.27

TABLE 5 Fragmentation Test Data at Increments of Applied Strain for the Plasma Poly(acrylic acid-co-1,7-octadiene) Coated and Untreated-unsized (HTA-5000) Fibres

Fragmentation test results	Acrylic acid (mole fraction)	Applied strain (%) 3	4	5	6	7	8	9	10
Number of fragments per 10 mm	0	5 ± 2	9 ± 1	10 ± 1	10 ± 1	10 ± 1	10 ± 1	10 ± 1	10 ± 1
	0.50	4 ± 1	9 ± 3	11 ± 1	12 ± 1	12 ± 1	12 ± 1	12 ± 1	12 ± 1
	0.75	7 ± 6	18 ± 2	19 ± 3	19 ± 3	19 ± 3	19 ± 3	19 ± 3	19 ± 2
	1	7 ± 4	20 ± 2	23 ± 2	24 ± 3	24 ± 4	24 ± 4	24 ± 5	24 ± 5
	Untreated	6 ± 4	16 ± 8	20 ± 5	22 ± 4	22 ± 4	22 ± 4	22 ± 4	22 ± 4
Average fragment length (mm)	0	2.30 ± 1.03	1.09 ± 0.11	1.03 ± 0.08	1.02 ± 0.07	1.02 ± 0.07	1.01 ± 0.08	1.01 ± 0.08	1.01 ± 0.08
	0.50	2.62 ± 1.65	1.29 ± 0.50	0.88 ± 0.07	0.87 ± 0.10	0.87 ± 0.10	0.87 ± 0.10	0.87 ± 0.10	0.87 ± 0.10
	0.75	2.50 ± 1.56	0.58 ± 0.08	0.54 ± 0.07	0.54 ± 0.07	0.54 ± 0.07	0.54 ± 0.07	0.54 ± 0.07	0.54 ± 0.06
	1	1.60 ± 0.46	0.50 ± 0.05	0.44 ± 0.05	0.43 ± 0.06	0.43 ± 0.06	0.43 ± 0.07	0.43 ± 0.07	0.43 ± 0.07
	Untreated	1.8 ± 1.65	1.01 ± 1.05	0.52 ± 0.15	0.46 ± 0.08	0.46 ± 0.08	0.46 ± 0.08	0.46 ± 0.08	0.46 ± 0.08
Degree of debonding (%)	0	100	100	100	100	100	100	100	100
	0.50	22.19 ± 10.20	37.42 ± 27.24	65.61 ± 4.03	69.34 ± 5.95	72.55 ± 6.19	75.26 ± 5.93	77.11 ± 4.23	78.98 ± 3.01
	0.75	2.07 ± 1.76	18.06 ± 7.46	29.28 ± 8.33	36.20 ± 9.02	39.47 ± 9.82	42.40 ± 10.53	44.75 ± 11.60	47.45 ± 12.33
	1	0.29 ± 0.46	6.91 ± 6.04	11.88 ± 9.01	16.13 ± 11.8	19.91 ± 14.1	23.08 ± 16.6	25.12 ± 17.0	28.06 ± 18.5
	Untreated	1.02 ± 1.07	13.44 ± 9.05	23.06 ± 9.29	33.10 ± 7.11	38.95 ± 5.61	43.21 ± 4.69	46.00 ± 5.05	49.10 ± 5.32
IFSS value (MPa)	0	7.16 ± 3.92	15.28 ± 2.00	16.33 ± 1.62	16.57 ± 1.52	16.57 ± 1.52	17.97 ± 16.70	17.97 ± 16.70	17.97 ± 16.70
	0.50	5.20 ± 0.83	14.00 ± 6.76	20.23 ± 2.04	20.62 ± 2.94	20.62 ± 2.94	20.62 ± 2.94	20.62 ± 2.94	20.62 ± 2.94
	0.75	10.89 ± 11.76	33.86 ± 5.53	37.10 ± 7.02	37.04 ± 6.78	37.04 ± 6.78	37.04 ± 6.78	37.04 ± 6.78	37.04 ± 6.78
	1	11.18 ± 7.90	36.91 ± 4.30	43.41 ± 5.48	44.92 ± 7.13	45.57 ± 8.52	45.71 ± 9.14	46.04 ± 9.76	46.75 ± 11.26
	Untreated	7.37 ± 8.12	29.16 ± 17.03	39.21 ± 12.59	43.52 ± 9.40	43.8 ± 9.63	43.63 ± 9.81	43.51 ± 9.93	43.15 ± 9.72
CSTF value (MPa)	0	201 ± 13	240 ± 10	286 ± 11	328 ± 13	364 ± 16	397 ± 19	430 ± 21	459 ± 24
	0.50	128 ± 14	248 ± 106	243 ± 52	263 ± 43	276 ± 26	300 ± 28	310 ± 36	331 ± 17
	0.75	728 ± 74	518 ± 79	456 ± 107	406 ± 98	389 ± 90	378 ± 89	374 ± 88	370 ± 86
	1	841 ± 66	665 ± 79	576 ± 67	527 ± 75	492 ± 81	472 ± 82	457 ± 83	445 ± 81
	Untreated	775 ± 182	560 ± 78	467 ± 126	370 ± 52	334 ± 34	313 ± 37	305 ± 43	294 ± 51

Average fibre tensile stress for elastic-elastic stress analysis. $\bar{\sigma}_f$ (MPa)	0	5971	7962	9987	12009	14010	16012	18013	20015
	0.50	5647	7455	9294	11181	13040	14896	16107	18603
	0.75	5177	6730	8524	10245	11964	13682	15512	17119
	1	5469	6699	8111	9647	11191	12668	14174	15870
	Untreated	5580	6803	8289	9800	11573	13089	14751	16478
SD in $\bar{\sigma}_f$	0	82	65	24	23	27	31	35	38
	0.50	168	150	274	316	356	392	466	501
	0.75	473	544	478	552	648	735	837	835
	1	300	170	333	503	698	1067	1438	1295
	Untreated	287	509	559	614	724	839	943	1030
STE	0	0.034 ± 0.002	0.031 ± 0.001	0.030 ± 0.001	0.028 ± 0.001	0.027 ± 0.001	0.026 ± 0.001	0.025 ± 0.001	0.024 ± 0.001
	0.50	0.023 ± 0.002	0.034 ± 0.015	0.027 ± 0.006	0.024 ± 0.005	0.021 ± 0.003	0.020 ± 0.002	0.019 ± 0.002	0.019 ± 0.002
	0.75	0.140 ± 0.010	0.075 ± 0.010	0.050 ± 0.010	0.038 ± 0.010	0.032 ± 0.007	0.027 ± 0.006	0.024 ± 0.005	0.021 ± 0.005
	1	0.154 ± 0.005	0.100 ± 0.011	0.072 ± 0.010	0.055 ± 0.010	0.045 ± 0.010	0.038 ± 0.010	0.033 ± 0.009	0.029 ± 0.007
	Untreated	0.150 ± 0.010	0.080 ± 0.010	0.056 ± 0.010	0.037 ± 0.010	0.029 ± 0.003	0.024 ± 0.002	0.020 ± 0.002	0.018 ± 0.002

average fragment length and percent debonding with applied strain are shown graphically in Figures 4, 5, and 6. It was found that the first fibre-break for all of the plasma-polymer-coated fibres appeared to occur at a strain of 2.2–2.7%. Therefore, a strain of 3% was chosen for the first measurement. As the strain increased, the fibres fragmented and the average fragment length decreased accordingly (Table 5, Figures 4 and 5). It was found that saturation in fragmentation occurred at an applied strain of 5% for the 0, 0.50, and 0.75 acrylic acid copolymer-coated fibres and a strain of 6% for the untreated fibres and those coated with plasma polyacrylic acid. At the first increment of strain at which measurements were taken, a small degree of debonding was already present at the fragment-ends of the fibres coated with acrylic acid plasma homopolymer ($0.29 \pm 0.46\%$), 0.75 acrylic acid plasma copolymer ($2.07 \pm 1.76\%$), and the untreated fibre ($1.02 \pm 1.07\%$), whereas significant debonding of $22.19 \pm 10.20\%$ and 100% was found for those coated with the 0.50 acrylic acid plasma copolymer and 1,7-octadiene plasma homopolymer, respectively. The degree of debonding increases with applied strain as presented in

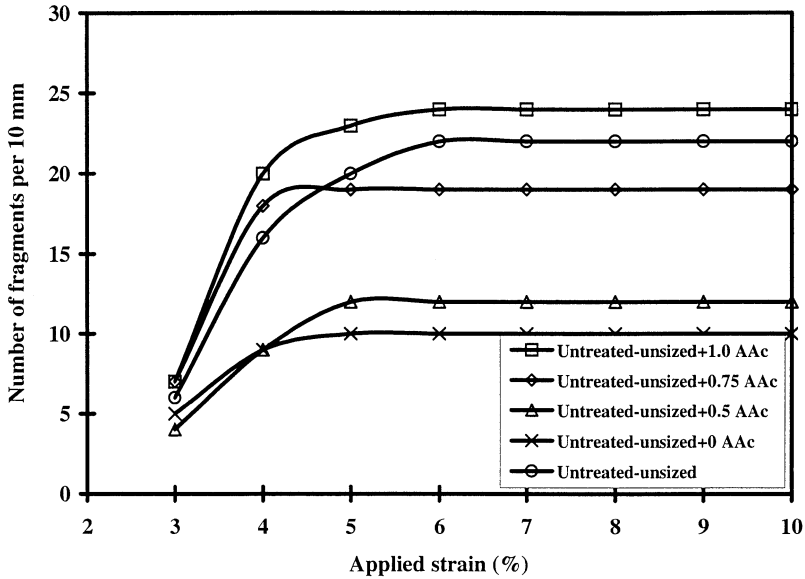

FIGURE 4 Variation in fragment number (number of fragments per 10 mm) as a function of applied strain for the plasma poly(acrylic acid-co-1,7-octadiene) coated at power of 5.0 W with varying mole fraction of acrylic acid (AAc) and untreated-unsized (HTA-5000) carbon fibres.

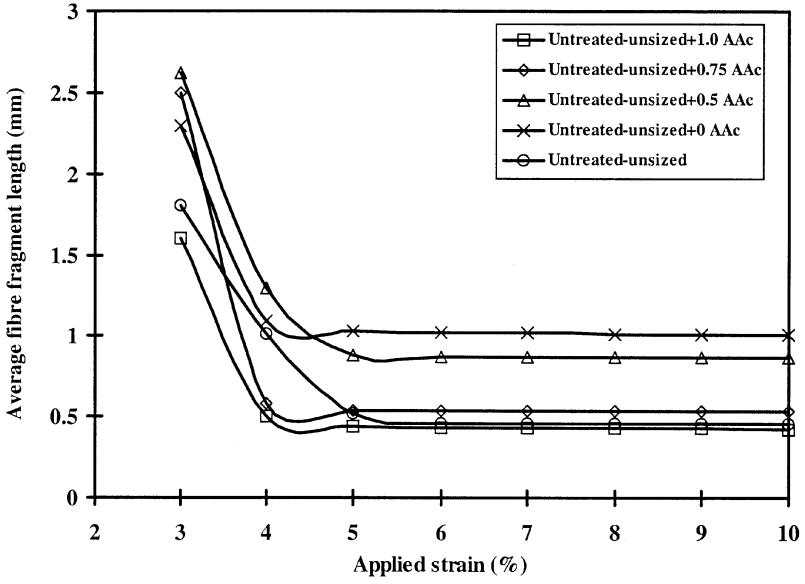

FIGURE 5 Variation in average fragment length as a function of applied strain for the plasma poly(acrylic acid-co-1,7-octadiene) coated at power of 5.0 W with varying mole fraction of acrylic acid (AAc) and untreated-unsized (HTA-5000) carbon fibres.

Figure 6. At a strain level of 10%, representative stress birefringence patterns associated with fibre-fracture, transverse matrix cracking, and interfacial debonding for the differing plasma-copolymer-coated fibres is given in Figure 6.

From Figure 7 it can be seen that with an increasing mole fraction of acrylic acid in the plasma feed the failure mechanism at fibre-fracture changes from interfacial debonding to a mixed mode, where debonds coexist with transverse matrix cracks. It can also be seen that the degree of debonding decreases, indicating that the fibre-matrix adhesion has increased. The fragmentation test data for the treated-unsized (HTA-5001), treated-sized (HTA-5131), and plasma-poly-acrylic-acid-coated, unsized, commercially-treated fibres are given in Table 6. The number of fragments/10 mm, average fragment length, and degree of debonding are presented graphically in Figures 8, 9, and 10. It has been found that the onset of fragmentation for treated-unsized fibres occurred at an applied strain slightly less than 2.0%, while for the treated-sized and untreated-unsized fibres fragmentation began at strains of 2.3% and 2.5–2.7%, respectively. The photoelastic

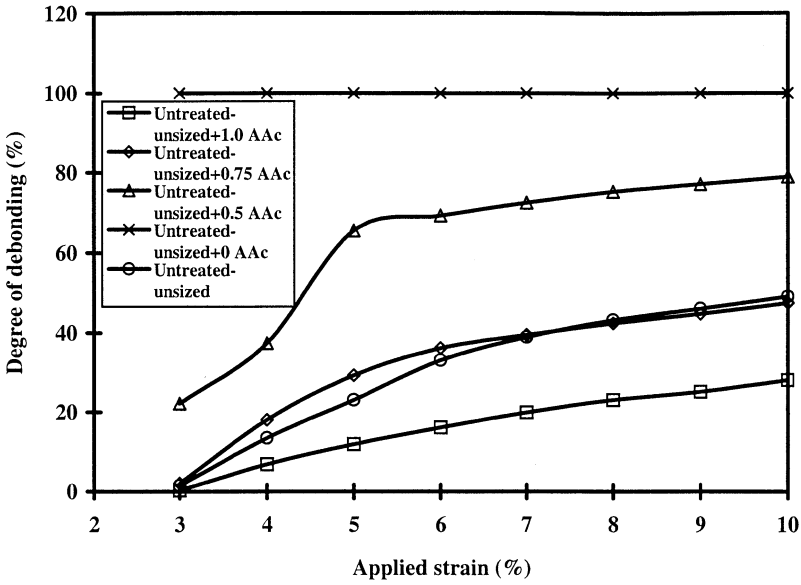

FIGURE 6 Variation in percent debonding as a function of applied strain for the plasma poly(acrylic acid-co-1,7-octadiene) coated at power of 5.0 W with varying mole fraction of acrylic acid (AAc) and untreated-unsized (HTA-5000) carbon fibres.

stress birefringence patterns at the fibre-breaks shown in Figure 11a and b are typical of transverse matrix cracking, which was observed for the treated-unsized and treated-sized fibres, respectively. It can be seen from Figure 10c that mixed-mode-failure was observed for the treated-unsized fibre coated with the acrylic acid plasma polymer, similar to the equivalent coating on an untreated-unsized fibre (Figure 7a). The degree of debonding for both acrylic acid plasma-polymer-coated fibres was also similar. This is indicative of similar interfacial strength after the plasma deposition, despite the higher concentration of carboxylic acid functional groups retained at lower power of 0.7 W compared with higher power of 5.0 W (Table 3). The implication of this result is that all of the reactive functional groups may not be involved in the formation of an adhesive bond.

As expected, the commercial oxidative surface treatment appears to have no effect on the adhesion of the coated fibres. This is consistent with the lower degree of adhesion (fully debonded) for the octadiene plasma-polymer-coated fibre (Figure 7d) and the assumption that the coating conceals the residual chemistry and the microporosity of the fibre

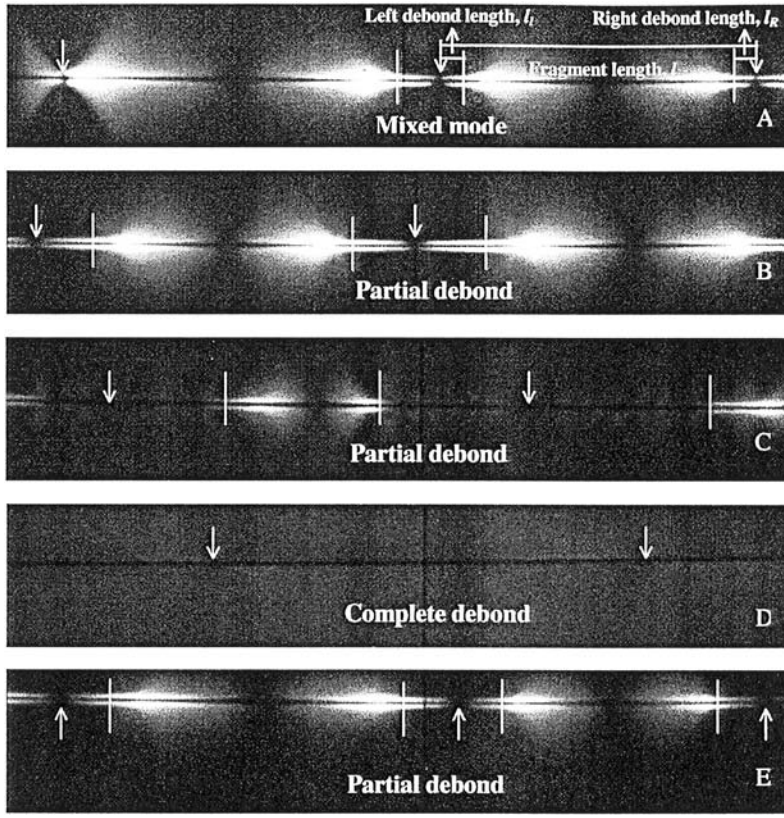

FIGURE 7 Polarized light micrographs showing stress birefringence pattern for the plasma poly(acrylic acid-co-1,7-octadiene) coated fibres at a power of 5.0 W with varying mole fraction of acrylic acid. From top to bottom: (A) 1.0, (B) 0.75, (C) 0.50, (D) 0, and (E) the untreated-unsized (HTA-5000) fibres in an epoxy matrix at saturation (applied strain of 10%). The arrow indicates a fibre-fracture, with the extent of the debonded region given by a vertical line.

surface. The comparison of the degrees of interfacial debonding shown in Table 7 indicates that the level of adhesion increases in the order of untreated-unsized $<$ acrylic acid plasma homopolymers $<$ treated-unsized $\approx$ treated-sized fibres. As the applied strain increased, the number of fibre-fractures increases and the average fragment length decreases. It was also observed that saturation was achieved at a lower strain (5–6%), with a higher average fragment length for the plasma-copolymer-coated fibres compared with the commercially-treated fibres (8%). This is because interfacial debonding was observed for the

TABLE 6 Fragmentation Test Data at Increments of Applied Strain for Treated-unsized (HTA-5001), Treated-sized (HTA-5131), and Plasma-polyacrylic-acid-coated-unsized, Commercially-treated Fibres

Fragmentation test results	Coating fibre	Applied strain (%)							
		3	4	5	6	7	8	9	10
Number of fragments per 10 mm	Treated-unsized	12 ± 4	24 ± 3	28 ± 3	30 ± 3	31 ± 3	33 ± 4	33 ± 4	33 ± 4
	Treated-sized	8 ± 3	21 ± 1	26 ± 0	28 ± 1	29 ± 1	30 ± 2	30 ± 1	30 ± 1
	Plasma polyacrylic acid/treated-unsized	7 ± 1	22 ± 2	25 ± 4	26 ± 4	26 ± 5	26 ± 2	26 ± 5	26 ± 5
Average fregment length (mm)	Treated-unsized	0.94 ± 0.42	0.42 ± 0.06	0.35 ± 0.03	0.34 ± 0.03	0.33 ± 0.03	0.32 ± 0.03	0.32 ± 0.03	0.31 ± 0.03
	Treated-sized	1.62 ± 0.88	0.47 ± 0.03	0.39 ± 0.01	0.37 ± 0.01	0.35 ± 0.01	0.34 ± 0.02	0.33 ± 0.02	0.33 ± 0.02
	Plasma polyacrylic acid/treated-unsized	1.50 ± 0.18	0.45 ± 0.05	0.40 ± 0.06	0.40 ± 0.07	0.40 ± 0.07	0.40 ± 0.07	0.40 ± 0.08	0.40 ± 0.08
Degree of debonding (%)	Treated-unsized	—	—	—	—	—	—	—	—
	Treated-sized	—	—	—	—	—	—	—	—
	Plasma polyacrylic acid/treated-unsized	0.90 ± 1.20	5.37 ± 7.80	8.73 ± 10.21	13.70 ± 13.63	17.33 ± 15.61	20.65 ± 16.85	23.96 ± 17.95	26.70 ± 18.21
IFSS value (MPa)	Treated-unsized	16.69 ± 5.98	38.61 ± 6.11	46.63 ± 5.43	48.88 ± 5.48	51.22 ± 5.89	52.89 ± 5.59	53.35 ± 5.95	54.08 ± 6.84
	Treated-sized	11.51 ± 6.02	39.06 ± 2.70	47.92 ± 1.18	51.82 ± 1.72	54.50 ± 2.68	56.47 ± 3.92	58.50 ± 4.19	58.50 ± 4.19
	Plasma polyacrylic acid/treated-unsized	9.40 ± 1.45	39.68 ± 5.24	45.46 ± 7.98	46.88 ± 9.47	46.88 ± 9.47	46.88 ± 9.47	47.19 ± 10.53	46.67 ± 9.81
CSTF value (MPa)	Treated-unsized	834 ± 11	694 ± 62	624 ± 49	599 ± 46	576 ± 43	563 ± 42	556 ± 49	550 ± 53
	Treated-sized	854 ± 30	748 ± 27	678 ± 12	638 ± 15	610 ± 20	601 ± 32	587 ± 28	586 ± 25
	Plasma polyacrylic acid/treated-unsized	835 ± 32	665 ± 69	588 ± 63	531 ± 73	503 ± 78	481 ± 77	462 ± 74	445 ± 70
Average fibre tensile stress for elastic-elastic stress analysis, $\bar{\sigma}_f$ (MPa)	Treated-unsized	5420	6369	7610	8935	10112	11423	12707	13994
	Treated-sized	5474	6677	7899	9139	10426	11844	13151	14607
	Plasma polyacrylic acid/treated-unsized	5537	6632	8004	9495	11069	12646	14219	15782

SD in $\bar{\sigma}_f$	Treated-unsized	52	101	67	175	186	263	458	597
	Treated-sized	116	136	98	132	109	228	187	177
	Plasma polyacrylic acid/treated-unsized	78	210	508	684	843	963	1135	1277
STE	Treated-unsized	0.160	0.110	0.083 ± 0.001	0.069 ± 0.001	0.058 ± 0.002	0.050	0.043 ± 0.002	0.039 ± 0.002
	Treated-sized	0.160 ± 0.006	0.110	0.087 ± 0.002	0.070	0.059 ± 0.001	0.051 ± 0.002	0.045 ± 0.002	0.040 ± 0.002
	Plasma polyacrylic acid/treated-unsized0.006	0.150 ± 0.010	0.10 ± 0.013	0.076 ± 0.010	0.057 ± 0.010	0.047 ± 0.010	0.041 ± 0.008	0.033 ± 0.007	0.030 ± 0.006

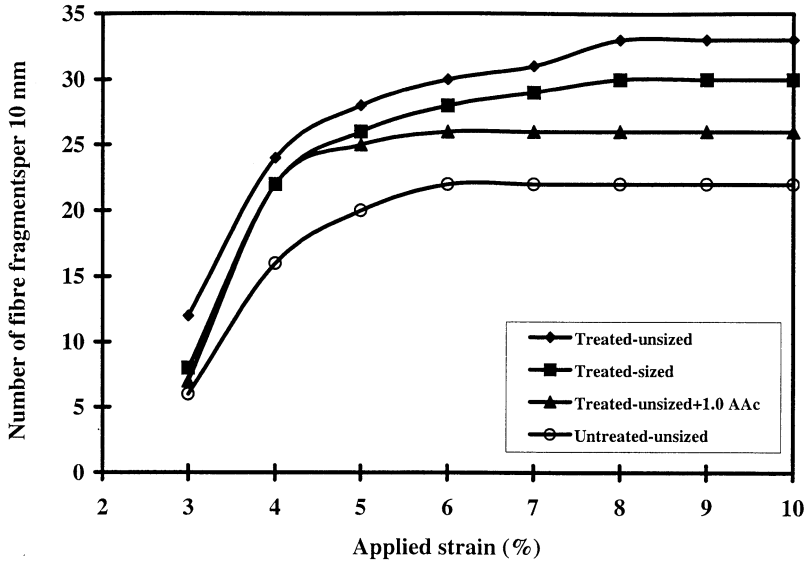

FIGURE 8 Variation in fragment number (number of fragments per 10 mm) as a function of applied strain for the treated-unsized (HTA-5001), treated-sized (HTA-5131), plasma-polyacrylic-acid-coated-unsized, commercially-treated (at power of 0.7 W), and untreated-unsized (HTA-5000) carbon fibres.

plasma-copolymer-coated fibres, thus effectively decreasing the bonded length for transfer stress and further fibre-fracture.

DISCUSSION

Surface Chemistry of Plasma Polymer Coated Fibres

The XPS results given in Table 3 show that the chemical functional groups deposited from the introduction of acrylic acid into the plasma feed predominantly appear in the form of COOR functional groups. The decreased concentration of this functional group is associated with the increase in percent C-C functionality when the mole fraction of hydrocarbon is increased. This indicates that the hydrocarbon is incorporated into the plasma polymer films. At low-plasma-power to monomer-flow-rate ratio, it has been shown by secondary ion mass spectrometry (SIMS) and XPS that most of the COOR functional groups correspond to carboxylic acid (COOH) [24, 25], while at high power a considerable fraction of this functional group has been shown to be ester (COOR) groups. As the total monomer flow rate was

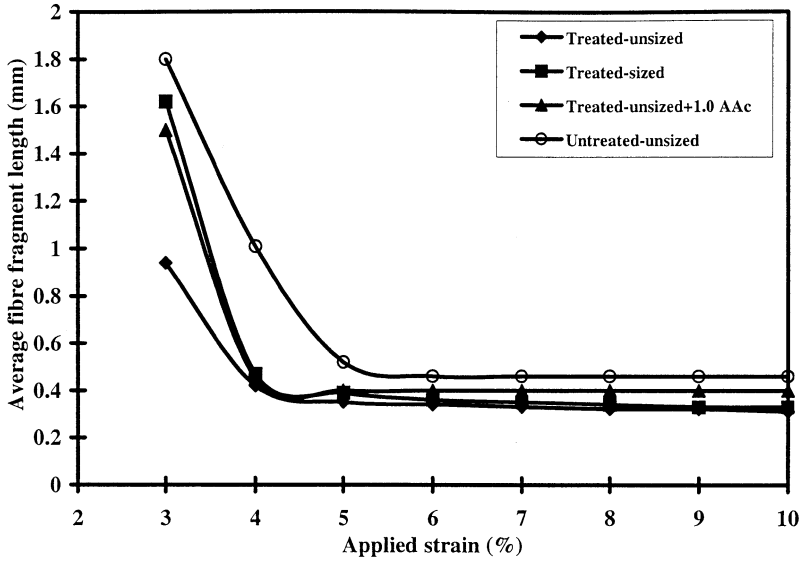

FIGURE 9 Variation in average fragment length as a function of applied strain for the treated-unsized (HTA-5001), treated-sized (HTA-5131), plasma-polyacrylic-acid-coated-unsized, commercially-treated (at power of 0.7 W), and untreated-unsized (HTA-5000) carbon fibres.

maintained to be constant (1.5 sccm), it was found that the percent carboxylate (COOR) groups retained at 0.7 W for the acrylic acid plasma polymer is of the same magnitude as those formed at 5.0 W. This is because the relative concentrations of COR and C=O functional groups indicate that the COOR groups formed at 0.7 W are predominantly carboxylic acid groups, while at 5.0 W concentration of ester groups is higher. This arises from the difference in energy input which results in dissociation of acrylic acid (C-O bond) rather than the polymerization of acrylic acid through the double bond (C=C) [26]. Similar observations have been noted by O'Toole et al. [27] and Candan et al. [28].

Tensile Strength of Plasma Polymer Coated Fibres

The trend in Weibull modulus after polymer coating shown in Table 4 shows that the fibre strength is less variable in the presence of the plasma polymer coating layer. The statistics in strength-distribution within carbon fibres is connected to the variation in imperfections such as voids, flaws, and cracks within the fibre and on the surface. Coating

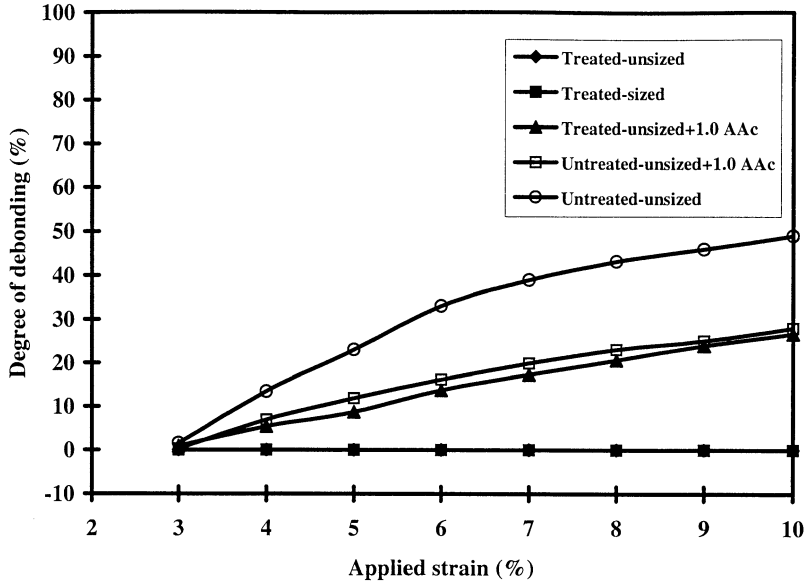

FIGURE 10 Variation in percent debonding as a function of applied strain for the treated-unsized (HTA-5001), treated-sized (HTA-5131), plasma-polyacrylic-acid-coated-unsized, commercially-untreated (at power of 0.7 W), plasma-polyacrylic-acid-coated-unsized, untreated (at a power of 5.0 W), and untreated-unsized (HTA-5000) carbon fibres.

the fibres with a polymer is known to provide protection to the fibres from the introduction into the surface of strength-reducing flaws. Since the filaments were coated while supported on a frame, and transferred directly to the card support for filament strength testing, it seems unlikely that stronger filaments have been selected for coating compared with those tested directly. Therefore, the interesting observation, that the more polar the plasma polymer the greater the improvement, may be significant. This could be attributed to the plasma polymer coatings penetrating the surface flaws to provide healing or protection from damage, which is influenced by the higher degree of adhesion. In the case of the plasma polymer octadiene, the low Weibull modulus for fibre strength-distribution could reflect a weaker bond between the fibre surface and the coating. Carbon fibres with plasma polymer coatings having higher strengths have been reported previously [9–11]. The treated-unsized fibres had strength comparable with that of the untreated fibres, despite the fact that they have been manufactured in different batches. Baillie and Bader [30] reported the effect of electrolytic oxidation and showed that both the

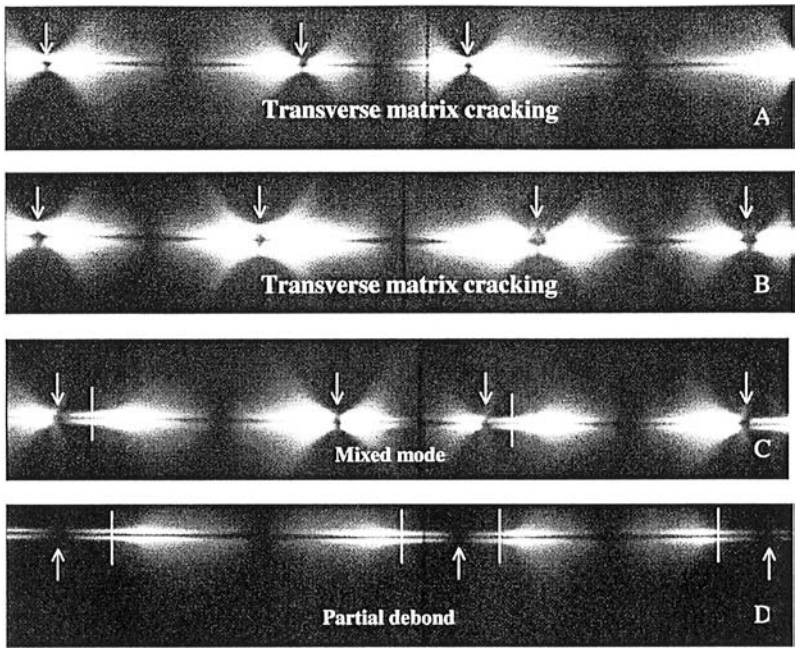

FIGURE 11 Polarized light micrograph showing stress birefringence pattern for (A) the treated-unsized (HTA-5001), (B) treated-sized (HTA-5131), (C) the plasma-polyacrylic-acid-coated-unsized, commercially-treated (HTA-5001) (at 0.7 W), and (D) untreated-unsized (HTA-5000) carbon fibres in an epoxy matrix at saturation (applied strain of 10%). The arrow indicates a fibre-fracture with the extent of the debonded region given by a vertical line.

TABLE 7 Ranking of Adhesion for the Plasma Poly(acrylic acid-co-1,7-octadiene) Coated and Untreated-unsized (HTA-5001) Carbon Fibres

Acrylic acid (mole fraction)	Fragment number/ 10 mm (applied strain of 6%)	Degree of debonding (%)	CSTF (applied strain of 6%)	STE at constant length	IFSS (applied strain of 6%)
0	5	5	4	5	5
0.50	4	4	5	4	4
0.75	3	2	2	3	3
1.0	1	1	1	1	1
Untreated-unsized	2	2	2	2	2

fibre-strength and Weibull modulus were increased. This was considered to result from the removal of surface defects during oxidation. The treated-sized fibres exhibited the highest strength and Weibull modulus, which demonstrates the benefit of immediately sizing the fibres after spinner and surface treatment.

The Assessment of Interfacial Adhesion

All of these untreated carbon fibres, with and without plasma polymer coating, exhibited debonding at fragment ends during continuous monitoring of the fragmentation. Neither of the electrolytically oxidized or treated fibres, with and without polymer size, exhibited debonding after fibre fracture. This is because yielding, within the matrix or, for the sized fibres, in the interphase, had occurred. We have previously demonstrated that yielding rather than debonding can influence the stress transfer back into the fibre at a break [2, 17]. The plasma polymer coatings employed here are of a thickness of 200–300 nm (Figure 3). They are highly cross-linked polymers and as a result will have a modulus not dissimilar to the matrix and probably higher. In recent FE modelling studies [31, 32] with perfectly bonded fibres, yieldable coatings of this thickness have been shown to influence stress transfer. However, in these studies debonding was the main interfacial phenomenon observed, demonstrating that yielding in the plasma polymer interphase will not make a significant contribution. For the rankings, debonding was in excess of $\simeq 20\%$. Since with the octadiene plasma polymer coating the fibres are completely debonded, whereas the precursor, untreated fibres were only 40% debonded, it can be assumed that the interface which fails is the one between the coating and matrix. In this case any yield will be confined to the matrix so that the CSTF methodology can be applied.

Fibres Coated with Plasma Polymers of Acrylic Acid/1,7-Octadiene

The fragmentation of the plasma polyacrylic acid-co-1,7-octadiene coated fibres exhibited two trends in CSTF as shown in Figure 12, whereby it increased or decreased with the applied strain. As the fibre fractures, the average fragment length becomes smaller. This causes the CSTF value to decrease with strain, which is clearly seen in the case of 1.0, 0.75 acrylic acid plasma copolymer coated and the untreated-unsized fibres. As the fibre fragmentation reaches saturation, however, the CSTF continues to decrease because the interface debonds progressively. The CSTF values for these fibres can be used to rank the interfacial adhesion; the 0.75 $\approx$ the untreated fibre $<$ the 1.0

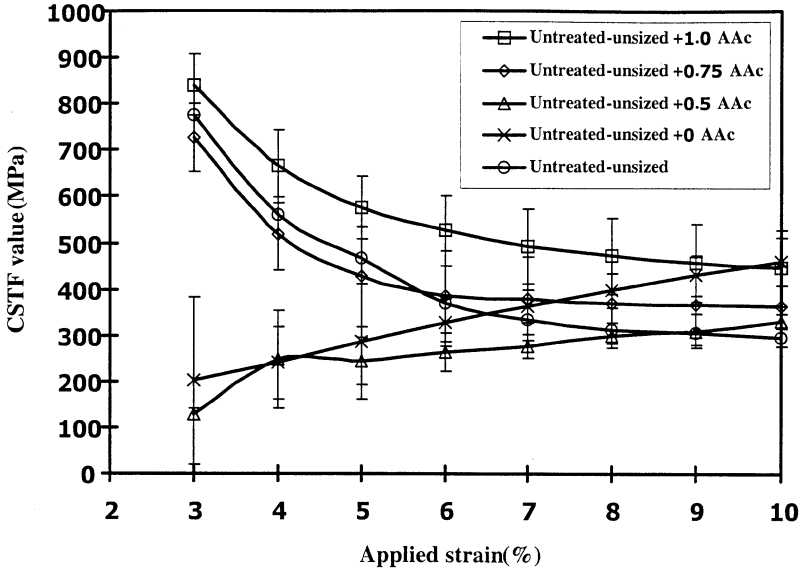

FIGURE 12 Variation in the CSTF as a function of applied strain for the plasma poly(acrylic acid-co-1,7-octadiene) coated at power of 5.0 W with varying mole fraction of acrylic acid (AAc) and the untreated-unsized (HTA-5000) carbon fibres.

acrylic acid plasma polymer coated fibres (Table 7). The improvement in adhesion for acrylic acid plasma homopolymer is consistent with that reported by Lopattananon et al. [8]. For the octadiene plasma polymer coated fibres, it has been found that saturation occurred simultaneously with complete debonding. This leads to the increasing trend in CSTF. A similar trend was also observed in the case of 0.5 acrylic acid plasma polymer coated fibres. In this case, the composite load becomes the only varying parameter for the calculation of CSTF. Therefore, CSTF increases as shown. This aspect can be removed from the analysis by calculating a stress transfer efficiency (STE) which gives a better discrimination between the differing degrees of interfacial adhesion, as shown in Figure 13.

From the values of stress transfer efficiency for all of the plasma polymer coated fibres, a ranking of interfacial adhesion at an applied strain of 6% can be obtained as shown in Table 7 ($0 < 0.5 < 0.75 \approx$ untreated-unsized $<$ 1.0 acrylic acid plasma polymer coatings). This is consistent with the degree of debonding shown in Figure 6.

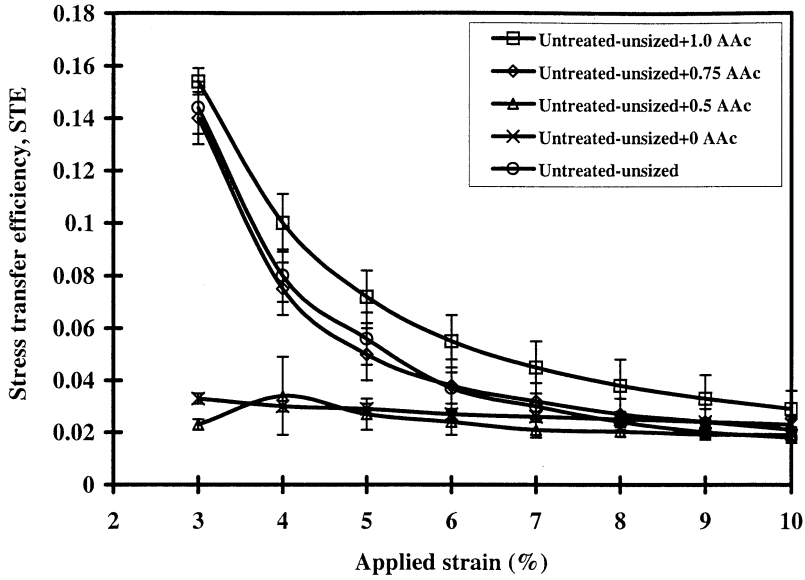

FIGURE 13 Variation in the STE as a function of applied strain for the plasma poly(acrylic acid-co-1,7-octadiene) coated at power of 5.0 W with varying mole fraction of acrylic acid (AAc) and untreated-unsized (HTA-5000) carbon fibres.

With the conventional analysis, the apparent interfacial shear strength reaches a plateau as a result of saturation in average fragment length as shown in Figure 14. The major assumption in the calculation of IFSS is that better adhesion leads to shorter fragments. Since there is no further reduction in average fragment length and saturation is reached below 6%, ranking in IFSS can be given (Table 7). However, the degree of debonding in Figure 6 is varying so that the validity of the constant shear model is in doubt. On the other hand, the low value of IFSS in the case of octadiene plasma polymer coating (18 ± 16 MPa) indicates that the interfacial bond strength is low. What is especially noticeable is that the ranking differs from that above, especially for the partially-debonded untreated-unsized and 0.75 acrylic acid coated fibres. In Table 7, CSTF and percent debonding rankings suggest very similar degrees of adhesion, but the IFSS and the fragment number clearly identifies the former as better. This analysis shows that debonding hardly influences the value of IFSS. The problem with STE and CSTF is that at the same applied strain the fragment length differs.

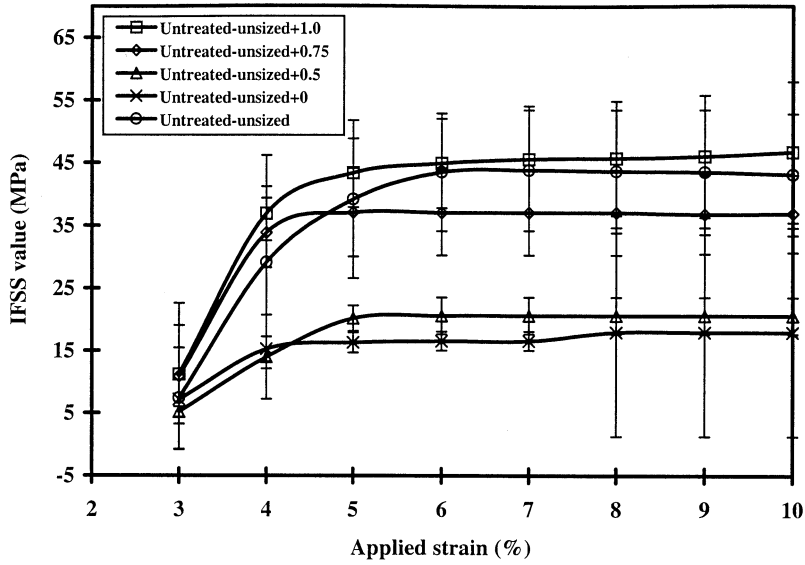

FIGURE 14 Variation in the IFSS as a function of applied strain for the plasma poly(acrylic acid-co-1,7-octadiene) coated at power of 5.0 W with varying mole fraction of acrylic acid (AAc) and untreated-unsized (HTA-5000) carbon fibres.

As shown in Figure 2, under ideal elastic conditions and in Figure 1b for debonded fibres in an elastoplastic matrix, the average stress transferred to a fibre-fragment is a function of the applied strain and its length. Therefore, a comparison of STE values at a constant applied strain could be misleading because the fragment lengths are not identical. Therefore, the change in STE against fragment length throughout fragmentation can be plotted. Figure 15 shows that the curve exhibits two regions: 1) at long fragment lengths dominated by the statistics of fibre fracture and 2) at short lengths dominated by stress transfer. It is clear from Figure 15 that it is not possible to compare the STE in region II at a constant average fragment length. The data are best represented as shown in Figure 16, as the shortest fragment with the highest STE. Thus, the fibres coated with the surface-functionalizing acrylic acid plasma polymer clearly have the highest level of adhesion. By comparing the data in this way the difference between the untreated-unsized fibre and 0.75 acrylic acid coated fibre can now be quantified. However, it is still not possible to compare the length at constant STE, and therefore an alternative histogram is not feasible either. We are exploring other extrapolation

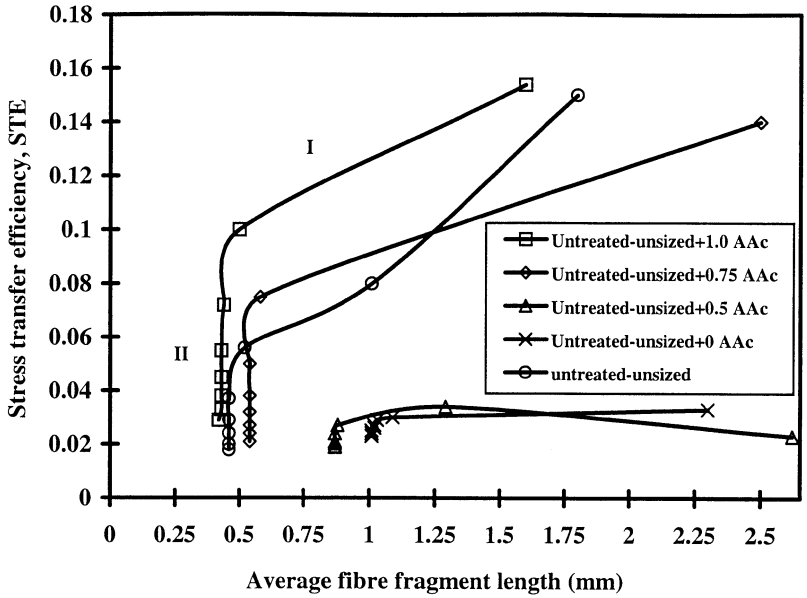

FIGURE 15 Plot of STE against average fragment length for the complete fragmentation process showing the change from type I to type II behavior.

procedures. Despite this, the ranking of all of the fibres is now in the same order as the interfacial shear strength (Table 7). This gives confidence to previous rankings based on the constant shear model. As shown in Figures 9–11, the sizing resin influences the fragmentation behavior of the commercial fibre. In this case, debonding was not observed and yielding of an interphase region could be responsible. We have therefore analyzed the data using the same methodology. However, current techniques do not allow the measurement of interphase properties and, besides, dissolution of a sizing resin will give a gradation in properties. For comparison we have assumed the matrix properties given in Table 1.

Commercially Treated Fibres

Figure 17 shows the variation of calculated CSTF with applied strain for the treated-sized, treated-unsized, and polyacrylic-acid-coated carbon fibres. As can be seen, the CSTF of these fibres decreases with increasing applied load because they are fragmenting into less efficient fibres. The treated-unsized and treated-sized fibres produce similar values of CSTF, suggesting that both fibres have

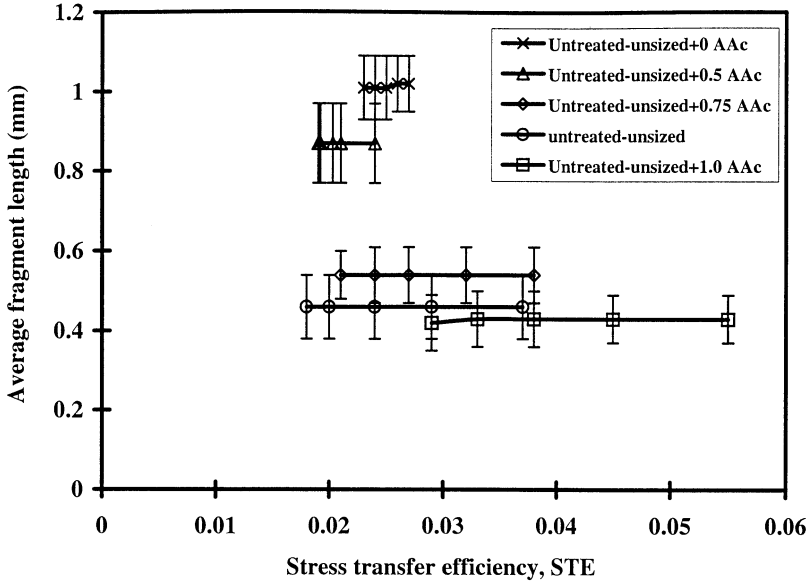

FIGURE 16 Variation in average fragment length in region II as a function of STE for the plasma poly(acrylic acid-co-1,7-octadiene) coated at power of 5.0 W with varying molar fraction of acrylic acid (AAc) and untreated-unsized (HTA-5000).

similar degrees of interfacial adhesion. Debonding was not observed in either case. However, when interfacial debonding occurs at fragment-ends, as with all of the plasma-polymer-coated and the untreated-unsized carbon fibres, CSTF decreases further. The acrylic acid plasma-polymer-coated treated and untreated fibres had similar values throughout the range of applied strain. The following ranking is inferred; untreated-unsized $<$ plasma polyacrylic acid $<$ treated-sized $\approx$ treated-unsized fibres (Table 8). The stress transfer efficiencies of the treated-sized and treated-unsized carbon fibres are compared with the plasma-polymer-coated equivalents as shown in Figure 18. The calculated values of IFSS for these fibres are shown in Figure 19. The fibres which debond achieve saturation during fragmentation while the treated-unsized and treated-sized fibres do not. Estimates of interfacial strength can still be made, and these are at 54 ± 7 and 58 ± 4 MPa for treated-unsized and treated-sized fibres, respectively. The average fragment length for the treated-unsized fibre is slightly less than that for the treated-sized fibre (Figure 8), but the calculated value of IFSS is apparently lower because of differences in

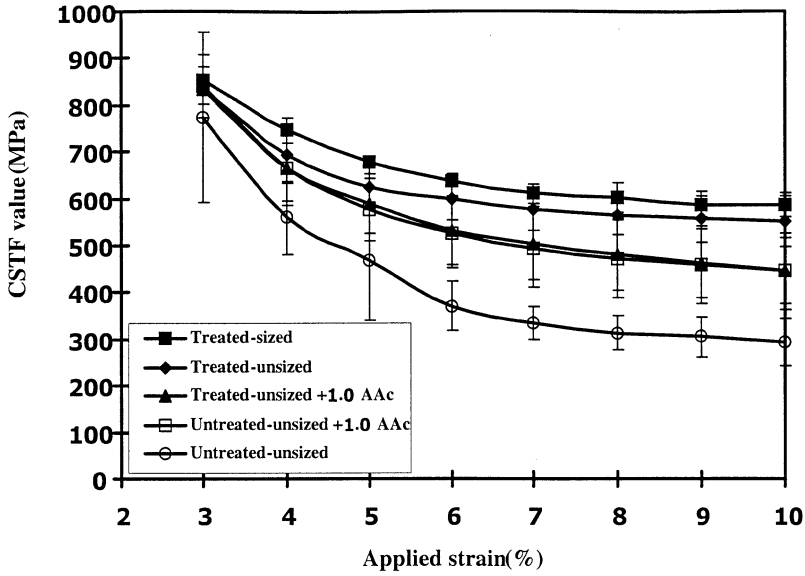

FIGURE 17 Variation in the CSTF as a function of applied strain for the treated-unsized (HTA-5001), treated-sized (HTA-5131), plasma-polyacrylic-acid-coated-unsized, commercially-treated (at power of 0.7 W), plasma-polyacrylic-acid-coated-unsized, untreated (at power of 5.0 W), and the untreated-unsized (HTA-5000) carbon fibres.

the tensile strength of the fibres. In the absence of debonding, matrix yielding can be expected as a result of the high shear stresses at the fibre-fracture. Thus, the validity of these values is brought into question.

For the treated-unsized and treated-sized carbon fibres, calibration curves similar to Figure 2 can be obtained. This can be used to convert CSTF to STE. The variation in STE with average fragment length is shown in Figure 20. One aspect of this analysis is the need to compare fibres under identical conditions. In Figure 9 the fragment length at the same applied strain differs in each case. Therefore, we have examined the STE of each fibre as a function of length (Figure 20). Figure 20 is clearly very important because by comparing the plots of STE against fragment length, we can see differences between the sized and unsized treated fibres and the two acrylic acid plasma-homopolymer-coated fibres. At the same STE the treated, unsized fibres have the smallest length. Therefore, the order of increasing adhesion is untreated < plasma polyacrylic acid < treated-sized < treated-unsized

TABLE 8 Ranking of Adhesion for Differently-sized Fibres: Treated-unsized (HTA-5001), Treated-sized (HTA-5131), Plasma-polyacrylic-acid-coated-unsized, Commercially-treated (HTA-5001), and Untreated-unsized (HTA-5000) Carbon Fibres

Fibre	Fragment number/10 mm (applied strain of 6%)	Degree of debonding (%)	CSTF (applied strain of 6%)	STE at constant length	IFSS (applied strain of 6%)
Treated-unsized	1	1	2	1	2
Treated-sized	2	1	1	2	1
Plasma-polyacrylic-acid-coated-unsized, treated	3	3	3	3	3
Untreated-unsized	4	4	4	4	4

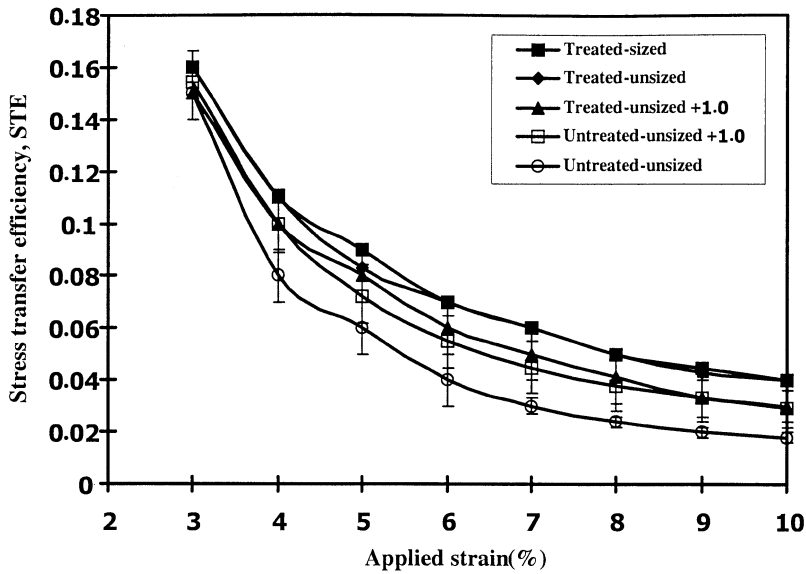

FIGURE 18 Variation STE as a function of applied strain for the treated unsized (HTA-5001), treated-sized (HTA-5131), plasma-polyacrylic-acid-coated-unsized, commercially-treated (at power of 0.7 W), plasma-polyacrylic-acid-coated-unsized, untreated (at power of 5.0 W), and the untreated-unsized (HTA-5000) carbon fibres.

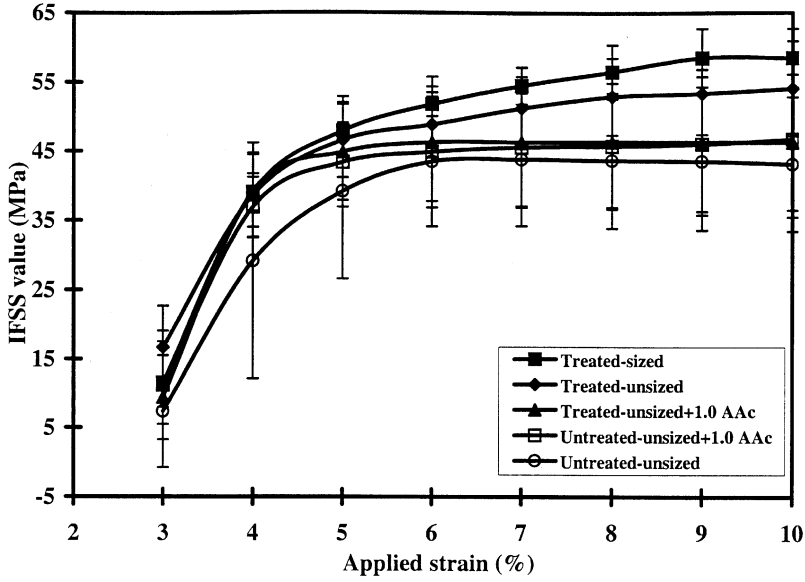

FIGURE 19 Variation in the IFSS as a function of applied strain for the treated-unsized (HTA-5001), treated-sized (HTA-5131), plasma-polyacrylic-acid-coated-unsized, commercially-treated (at power of 0.7), plasma-poly-acrylic-acid-coated-unsized, untreated (at power of 5.0 W), and the untreated-unsized (HTA-5000) carbon fibres.

fibre (Table 8). Thus, the sizing resin has the effect of slightly reducing the STE, which may be attributed to the formation of an interphase of lower yield strength. This result is similar to the observation of Cheng et al. [2]. However, in the constant shear analysis IFSS (Figure 19) τ is slightly larger for the sized fibres, suggesting that a higher degree of adhesion exists. Since debonding did not occur in either case the differences can only be attributed to yielding in the interphase region. Consideration of the fragment number alone would lead to the incorrect conclusion that the interphase had a higher modulus [1].

For the plasma polymer coatings employed here debonding occurred in every case, so interphasal yield cannot be significant. Therefore, the CSTF methodology can be used to calculate a STE from the fragmentation test data and provide a more self-consistent evaluation of "interfacial adhesion." It has been demonstrated that it is not necessary to reach saturation as required by the conventional analysis. Therefore, fibre-matrix interfaces can be examined, and

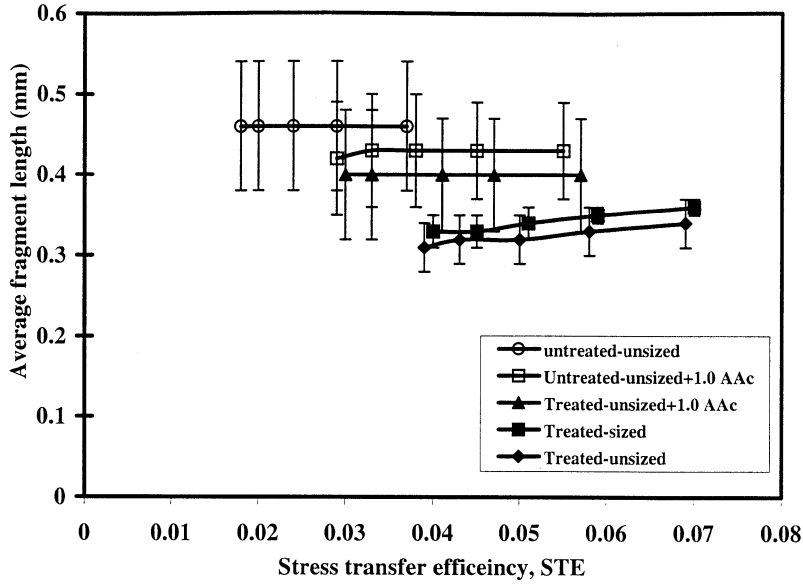

FIGURE 20 Variation in average fragment length as a function of STE for the treated-unsized (HTA-5001), treated-sized (HTA-5131), plasma-polyacrylic-acid-coated-unsized, commercially-treated (at power of 0.7), plasma-poly-acrylic-acid-coated-unsized, untreated (at power of 5.0 W), and the untreated-unsized (HTA-5000) carbon fibres.

model resins of high failure strain are not required. Furthermore, it is possible to determine a value for the STE when debonding does not occur. Thus, by comparing values of STE at a given fragment length we can differentiate between sized and unsized fibres and quantify the interfacial response where yielding occurs at the interface or within the interphase. What is especially noticeable is that the ranking differs from that above, especially for the partially debonding untreated-unsized and 0.75 acrylic acid-coated fibres. CSTF and percent debonding suggest very similar degrees of adhesion, but IFSS and fragment number clearly identify the former as better. This analysis has identified problems with STE and CSTF whereby the fragment length differs at the same applied strain. However, this can be overcome by comparing fragments of similar length. On the other hand, the problem with IFSS is that partial debonding does not appear to have an influence on the ranking, and the calculated values are not suitable for incorporation into other models.

CONCLUSION

Radio-frequency-induced plasma polymerization of acrylic acid/1,7-octadiene gas mixtures was applied to Type A carbon fibres to produce a varying range of carboxylic-acid-group-containing coatings. The single-fibre fragmentation test has been used to assess the interfacial adhesion of these plasma-polymer-coated fibres to epoxy resin. The cumulative stress transfer function (CSTF) and the conventional data Kelly-Tyson methodologies have been used to analyze the data. By visual examination of the fibre-fragmentation process at increments of applied strain, the number of fibre-fractures and degree of debonding at the interface was measured. The CSTF was found to provide a more self-consistent analysis of the interface performance, enabling differences between surface treatment and sizing to be evaluated. It was possible to quantify the response well below saturation. The degree of debonding was a good measure of the relative interface/interphase adhesive strength. An increase in mole fraction of acrylic acid in the plasma feed from $0 < 0.5 < 0.75 < 1.0$ led to a decrease in the degree of debonding. The untreated-unsized fibre was found to exhibit a degree of debonding similar to that of 0.75 acrylic acid plasma-polymer-coated fibre. The deposition of plasma copolymer films onto the carbon fibres also resulted in a reduction in the breadth of fibre-strength distribution, as indicated by an increase in Weibull modulus.

Where debonds propagate from fibre-fractures with strain (0.75 and 1.0 acrylic acid plasma-polymer-coated and untreated-unsized carbon fibres), the CSTF and the degree of debonding show similar trends. However, with 0 and 0.5 acrylic acid plasma-polymer-coated fibres, where full debonding occurred before the fragmentation test was complete, CSTF value continued to rise. However, when normalized into a stress transfer efficiency (STE) a good quantitative measure of interface quality over all of the surface treatments and coatings was achieved. Since CSTF and STE are a function of length, the STEs at similar fragment lengths have also been compared. Unfortunately, not all of the fibres could be compared in this way, and it is better to identify the best "adhesion" as the fibre with the shortest length and highest STE value. In this way, the requirement for the determination of fibre-strength (as required in the conventional analysis) can also be removed.

A comparative analysis of the data by the Kelly-Tyson model showed that it could be used to rank the differing degrees of adhesion when debonding dominated the micromechanics, despite being insensitive to debonding but sensitive only to fragment length or number. However, when good adhesion existed, it was insensitive to

the effects of sizing resin. The STE, on the other hand, could be used to quantify the influence of interphase formation.

Whether the plasma polymer was on the untreated-unsized or treated-unsized carbon fibres, there was little effect on STE. The improvement in adhesion of the fibres coated with plasma polyacrylic acid-co-1,7-octadiene (at saturation strain of 6%, Table 8) correlated well with the increase in concentration of carboxylic acid groups. This could be attributed to the formation of covalent bonds between the fibre surface and the epoxy resin, because the nonacrylic-acid-containing coating provided a lower degree of adhesion to the matrix than that for the untreated fibre.

With commercially-treated carbon fibres, the values of CSTF and STE were also shown to be consistent with the change in failure mode after surface treatment. These electrolytically oxidized carbon fibres exhibited improved stress transfer ability over their untreated counterparts, presumably because of the introduction of chemically-active functional groups such as carboxylic acid [3].

However, the deposition of a sizing resin onto the treated carbon fibres appeared to increase the level of adhesion according to CSTF and IFSS values, but the STE at a "constant length" demonstrated that a reduced efficacy existed, since it is assumed that yielding within the interphase region had occurred. Furthermore, fragmentation did not reach saturation so that the application of the "constant shear analysis" can be considered to be invalid.

Alternative energy-based techniques (e.g., Wagner et al. [33]) attempt to calculate an energy release rate from the rate of debonding and therefore can only be applied to debondable interfaces. On the other hand, the CSTF methodology has been shown to provide a quantification of interfacial response which can be applied equally to debondable and non debondable interfaces.

REFERENCES

[1] L. T. Drzal, J. M. Rich, M. F. Koenig, and P. F. Lloyd, *J. Adhesion*, **16**, 133 (1983).
[2] T. H. Cheng, J. Zhang, S. Yumitori, F. R. Jones, and C. W. Anderson, *Composites*, **25**, 661 (1994).
[3] P. Denison, F. R. Jones, and J. F. Watts, X-ray photoelectron spectroscopic analysis of barium-labelled carbon fibre surfaces, *J. Mater. Sci.*, **20**, 4647 (1985).
[4] E. Fitzer and R. Weiss, *Carbon*, **25**, 455 (1987).
[5] M. Guigon and E. Klinklin, *Composites*, **25**, 534 (1994).
[6] P. Denison, F. R. Jones, G. Dorey, L. F. Jones, and J. F. Watts, *Carbon'88*, B. McEnaney, and T. J. Mays, Eds. London: IOP Publishing, Institute of Physics (1988), pp. 634–636.
[7] L. T. Drzal, M. J. Rich, and P. F. Lloyd, *J. Adhesion*, **16**, 1 (1982).

[8] N. Lopattananon, A. P. Kettle, D. Tripathi, A. J. Beck, R. M. Duval, R. D. Short, and F. R. Jones, *Composites A*, **30**, 49 (1998).
[9] G. Dangli and N. H. Sung, *Polym. Comp.*, **10**, 109 (1989).
[10] N. Dilsiz, E. Ebert, W. Weisweiler, and G. Akovali, *J. Colloid Interf. Sci.*, **170**, 241 (1995).
[11] G. Akovali and N. Dilsiz, *Polym. Eng. Sci.*, **36**, 1081 (1996).
[12] L. T. Drzal and M. Madhukar, *J. Mater. Sci.*, **28**, 569 (1993).
[13] W. A. Frazer, F. H. Ancher, A. T. Dibenedetto, and B. Elbirli, *Polym. Comp.*, **4**, 238 (1983).
[14] A. Kelly and W. R. Tyson, *J. Mech. Phys. Solids.*, **13**, 329 (1965).
[15] P. Feillard, G. Désarmot, and J. P. Favre, *Comp. Sci. Technol.*, **49**, 109 (1993).
[16] D. Tripathi and F. R. Jones, *J. Mater. Sci.*, **33**, 1 (1998).
[17] D. Tripathi and F. R. Jones, *Comp. Sci. Technol.*, **57**, 925 (1997).
[18] T. Ohsawa, A. Nakyama, M. Miwa, and A. Hasegawa, *J. Appl. Polym. Sci.*, **22**, 3203 (1978).
[19] D. Tripathi, F. Chen, and F. R. Jones, *J. Comp. Mater.*, **30**, 1514 (1996).
[20] J. Nairn, *Mech. Mater.*, **13**, 131 (1992).
[21] D. Tripathi, F. Chen, and F. R. Jones, *Pro. R. Soc. Lond.*, **A452**, 621 (1996).
[22] A. P. Kettle, A. J. Beck, L. O. O'Toole, F. R. Jones, and R. D. Short, *Comp. Sci. Technol.*, **57**, 1023 (1997).
[23] D. Tripathi, N. Lopattananon, and F. R. Jones, *Composites A.*, **29**, 1099 (1998).
[24] M. R. Alexander and T. M. Duc, *J. Mater. Chem.*, **8**, 937 (1998).
[25] L. O'Toole, A. J. Beck, and R. D. Short, *Macromolecules*, **29**, 5172 (1996).
[26] D. L. Cho, P. M. Claesson, and C.-G. Golander, *J. Appl. Polym. Sci.*, **41**, 1373 (1990).
[27] L. O'Toole, A. J. Beck, A. P. Ameen, F. R. Jones, and R. D. Short, *J. Chem. Soc. Faraday. Trans.*, **91**, 3907 (1995).
[28] S. Candan, A. J. Beck, L. O'Toole, and R. D. Short, *J. Vac. Sci. Technol.*, **16A**, 1702 (1998).
[29] S. C. Bennett, D. C. Johnson, and W. Johnson, *J. Mater. Sci.*, **18**, 3337 (1983).
[30] C. A. Baillie and M. G. Bader, *Comp. Sci. Technol.*, **48**, 103 (1993).
[31] R. Lane, S. A. Hayes, and F. R. Jones, *Composite Interfaces* **6**, 425 (1999).
[32] S. A. Hayes, R. Lane, and F. R. Jones, *Composites A*, **32**, 379 (2001).
[33] H. D. Wagner, J. A. Nairn, and M. Detassis, *Appl. Comp. Mater.*, **2**, 107 (1995).